Nano impact

ZnO nanoparticles (NPs), one of the most common engineered nanomaterials, have been used widely in many fields. Thus the potential of their release into the environment and the subsequent impacts on the environment and human health have raised much concern. Plants provide a potential pathway for the transport of ZnO NPs in the environment and serve as an important route for their bioaccumulation in the human food chain. In the present study, a combination of microscopic and spectroscopic characterization techniques was used to investigate the uptake pathway, accumulation speciation, and cellular localization of ZnO NPs in maize. The results demonstrate that the majority of Zn taken up was derived from Zn^{2+} released from ZnO NPs and Zn accumulated in the form of Zn phosphate. ZnO NPs were observed mainly in the epidermis, a small fraction of ZnO NPs further entered the vascular system through the sites of the primary root-lateral root junction.
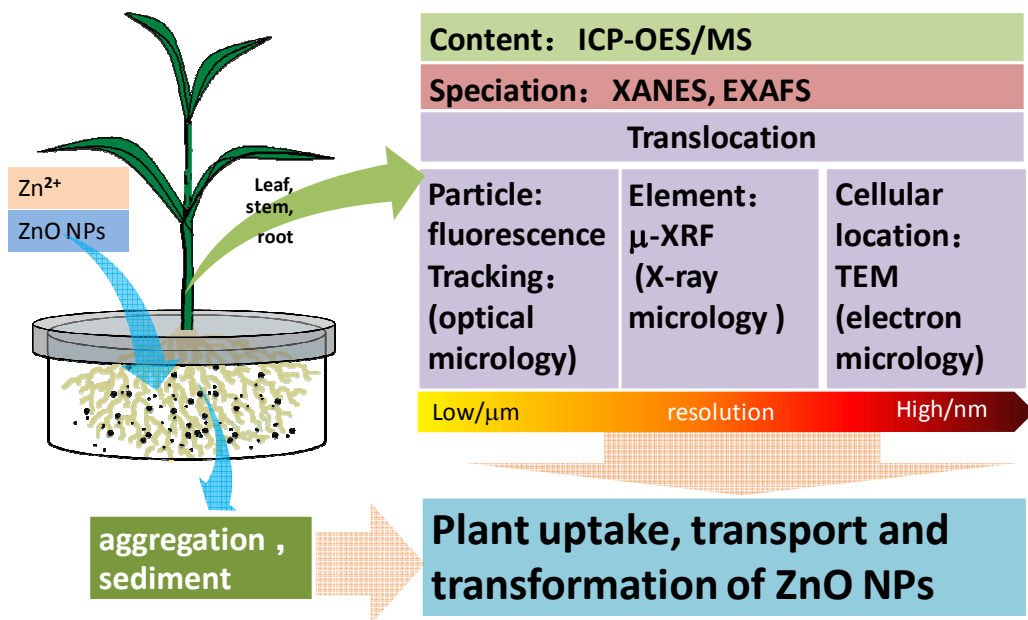
Graphical Abstract

1   **Accumulation, Speciation and Uptake Pathway of ZnO Nanoparticles in Maize**

2

3   Jitao Lv[a], Shuzhen Zhang[a*], Lei Luo[a], Jing Zhang[b], Ke Yang[c], Peter Christie[d]

4

5   [a] *State Key Laboratory of Environmental Chemistry and Ecotoxicology, Research*

6   *Center for Eco-Environmental Sciences, Chinese Academy of Sciences, Beijing*

7   *100085, China*

8   [b] *State Key Laboratory of Synchrotron Radiation, Institute of High Energy Physics,*

9   *Chinese Academy of Sciences, Beijing 100039, China*

10   [c] *Shanghai Institute of Applied Physics, Chinese Academy of Sciences, Shanghai,*

11   *201800, China*

12   [d] *Agri-Environment Branch, Agri-Food and Biosciences Institute, Newforge Lane,*

13   *Belfast BT9 5PX, United Kingdom*

14

15   [*]Corresponding author:

16   phone: +86-10-62849683;

17   fax: +86-10-62923563;

18   e-mail: szzhang@rcees.ac.cn.

19

20

Abstract

21

22 Engineered nanomaterials such as ZnO nanoparticles (NPs) will inevitably enter the

23 environment because of the large quantities produced and their widespread

24 application. Plants comprise a fundamental living component of terrestrial ecosystems,

25 thus understanding the interaction between ENMs and plants is important. In the

26 present study we conducted an integrated study by employing a combination of

27 microscopic and spectroscopic techniques to comparatively investigate the uptake of

28 ZnO NPs and Zn^{2+} ions by maize in order to further elucidate plant uptake pathways

29 of ZnO NPs. The results demonstrate that the majority of Zn taken up was derived

30 from Zn^{2+} released from ZnO NPs, and Zn accumulated in the form of Zn phosphate.

31 ZnO NPs were observed mainly in the epidermis, a small fraction of ZnO NPs were

32 present in the cortex and root tip cells, and some further entered the vascular system

33 through the sites of the primary root-lateral root junction. However, no ZnO

34 nanoparticle was observed to translocate to shoots, possibly due to the dissolution and

35 transformation of the ZnO NPs inside the plants.

36 **Keywords:** ZnO nanoparticles, Plant uptake, Pathway, Accumulation, Speciation,

37 Microscopic and spectroscopic observations

38

1. Introduction

The past decade has witnessed an exponential growth in nanotechnology with the manufacture of different types of engineered nanomaterials (ENMs) on a large scale for both industrial and household purposes. The potential for their release into the environment and subsequent impacts on the environment and human health has raised considerable concern.[1-3]

Plants comprise a fundamental living component of terrestrial ecosystems. Moreover, plant uptake, translocation and accumulation of ENMs may pose a threat to the safety of the human food chain.[4-6] However, plant uptake of ENMs is a very recent field of study and contradictory results have been reported, with some studies reporting plant accumulation of ENMs[7-8] and others showing no uptake.[9-13] Therefore, an attempt must be made to elucidate the pathways and mechanisms of NP uptake by plants to explain the contradictory observations regarding plant uptake. One of the most important distinguishing features of plant cells is that they are enclosed by rigid cell walls composed of cellulose, hemicelluloses and pectin with pores whose diameter is typically in the range 3-8 nm,[14] and these allow only small molecules to pass through. Navarro et al. therefore hypothesized that only nanoparticles with size smaller than the pores of cell walls can pass through and reach the plasma membrane.[5] However, many studies have shown that not only small NPs [12, 15-17] such as TiO_2, C_{70}, $C_{60}(OH)_{20}$ and Au with diameters < 5 nm, but also larger NPs were taken up by plant roots or even transported into the aerial parts of plants.[18-20] It is still unclear through which route the NPs pass through the cell walls and are internalized by plant cells to undergo vascular transport in plants, or how these particles pass though the Casparian strip, a belt of specialized cell wall material that generates an extracellular diffusion barrier around the vascular cylinder.[21] It is necessary to address

64   these important issues to elucidate the pathways and mechanisms of plant uptake and

65   translocation of NPs, which are still far from clear.[22]

66   ZnO NPs are amongst the most common engineered nanomaterials. They are used

67   widely in many applications, and consequently can be released into the

68   environment.[23] Research by Gottschalk et al. has indicated that the environmental

69   concentrations of ZnO NPs are second only to those of TiO_2.[24] This raises the urgent

70   need to understand the behaviors and effects of ZnO NPs in the environment.

71   Disposal of municipal solid wastes may provide an important pathway for plant

72   exposure to ZnO NPs due to the increasing commercialization of ENMs. Lin et al.

73   have studied the phytoaccumulation and phytotoxicity of ZnO nanoparticles at a

74   concentration of 1000 mg L^{-1} and observed the distribution of ZnO NPs in wheat roots

75   by transmission electron microscopy (TEM);[25] whereas Lopez-Moreno et al. reported

76   that there was no ZnO NP found in soybean (*Glycine max*) roots using synchrotron

77   X-ray absorption spectroscopy (XAS), even at a high concentration of ZnO NPs

78   (4000 mg L^{-1}).[26] Similarly, Hernandez-Viezcas et al. demonstrated that ZnO NPs were

79   not present in mesquite tissues, and Zn was found in a form resembling $Zn(NO_3)_2$.[13]

80   Recently, Hernandez-Viezcas et al. studied the location and speciation of ZnO and

81   CeO_2 nanoparticles taken up by Soybean (*Glycine max*) using micro X-ray

82   fluorescence analysis (μ-XRF) and micro X-ray absorption near-edge spectroscopy

83   (μ-XANES), and their results showed that Zn accumulated in a form resembling

84   Zn-citrate in soybean under treatment with ZnO NPs.[28] However, Zhao et al. studied

85   the uptake of (FITC)-stained ZnO NPs by corn plants growing in a sandy loam soil,

86   and they observed that ZnO NP aggregates penetrated root epidermis and cortex

87   through the apoplastic pathway, by using a confocal microscope. The presence of ZnO

88   NP aggregates in xylem vessels suggested that the aggregates passed the endodermis

89 through the symplastic pathway. [27] However, more information is necessary to

90 validate such conclusions, considering the limitations of confocal microscopy.

91 Moreover, although the uptake of ZnO NPs was involved in these studies, there are

92 still some questions needing to be further investigated. For example, whether Zn

93 accumulated in plants was from the uptake of ZnO NPs or Zn^{2+} ions was still unclear

94 since these studies lacked Zn^{2+} treatment as comparison. If the uptake of ZnO NPs by

95 plants exists, it is necessary to elucidate the route through which they enter plants and

96 in what form they accumulate in plants. Therefore, a combination of microscopic and

97 spectroscopic characterization techniques comprising synchrotron-based XAS and

98 μ-XRF analyses, optical fluorescence microscopic tracking of labeled ZnO NPs and

99 transmission electron microscopy (TEM) imaging was employed to investigate the

100 uptake pathway, accumulation, speciation, and cellular localization of ZnO NPs in

101 maize. The role of the dissolution of ZnO NPs in their uptake by maize was also

102 investigated in detail.

2. Materials and methods

2.1. Preparation of exposure suspension

105 The ZnO NPs were purchased from Nachen Scientific & Technical Co., Beijing,

106 China. The size distribution, crystal structure, surface charge, specific surface area

107 and aggregation state of ZnO NPs were measured, and the detailed methods are

108 provided in the Electronic Supplementary Information (ESI). Suspensions of ZnO

109 NPs were prepared at 0, 2, 5, 10, 15, 20, 40, 60, 80 and 100 mg L^{-1} (particle

110 concentration) in 1 % modified Hoagland solution stirred for 30 min, sonicated for 30

111 min, and then continuously stirred for 30 min to avoid sedimentation. $ZnSO_4$ at

112 various concentrations (Zn concentrations of 1, 1.5, 3, 6, 8, 10, 15, 20, 25, 30, 40, 50,

113 64 and 80 mg L^{-1}) dissolved in 1 % modified Hoagland solution was prepared for

114 plant exposure to Zn^{2+} in solution. The pH of each suspension was adjusted to 6.8 ±

115 0.2 before plant exposure. 10 ml of each ZnO NP suspension at various

116 concentrations was shaken at 100 rpm for 24 h at room temperature, aiming to detect

117 the dissolution of ZnO NPs. Then the dissolved Zn^{2+} and ZnO NPs were separated by

118 centrifuging at 20000 g for 40 min followed by filtration through 0.025 μm

119 microporous membranes (Millipore). The filtrates were acidified with 100 μL HNO_3

120 (pure) and quantified by ICP-OES (Optima 2000DV, Perkin Elmer). High quantitative

121 recovery of Zn^{2+} (96-100 %) was obtained by examining a series of solutions with

122 different soluble Zn^{2+} concentrations using the above procedure, indicative of

123 negligible retention of Zn^{2+} by the membrane. Therefore, the Zn present in filtrates

124 was considered as dissolved Zn released from ZnO NPs.

125 **2.2. Hydroponic cultivation and exposure experiments**

126 Maize (*Zea mays* L. cv. Zhengdan 958) was used as the test species. Seeds were

127 purchased from the Chinese Academy of Agricultural Sciences, Beijing, China.

128 Hydroponics was used for plant cultivation and exposure. The seedlings grew in 50 %

129 Hoagland nutrient solution for 7 d with 16 h d^{-1} simulated sunshine provided by

130 supplementary illumination (light intensity of 250 μmol m^{-2} s^{-1}) at a temperature of

131 25-30 °C, and a night (8 h) temperature of 15-20 °C before the exposure study (details

132 provided in the ESI). After 7 d of hydroponic cultivation, maize seedlings were

133 exposed to the ZnO NP suspensions or Zn^{2+} solutions described above. The exposure

134 suspensions or solutions were renewed daily and the exposure lasted for 7 d. After

135 plant exposure, the suspension pH showed only slight change (ranging from 6.6 to 7.2)

136 and no subsequent pH adjustments were then performed. The Zn^{2+} concentrations in

137 the filtrates (dissolved Zn^{2+}) of ZnO suspensions after plant exposure were separated

138 and measured by the same method as described above. Plant tissue samples were

139 lyophilized and then 0.1000 g samples were digested using HNO_3 and $HClO_4$ (4:1)

140 following the method of Yu et al.[29] Zn concentrations were then quantified by

141 ICP-OES. A tea standard reference material, GBW 10016 obtained from the Center of

142 National Standard Reference Material of China, was analyzed and good agreement

143 was achieved between the data obtained from the present work and the certified

144 values, with recoveries between 93 and 105%.

145 **2.3. Sample preparation for microscopy and μ-XRF analysis**

146 Fresh seedlings grown in 100 mg ZnO NPs L^{-1} or 30 mg Zn^{2+} L^{-1} solution for 7 d

147 were washed with deionized water three times and divided into roots, stems and

148 leaves. Samples were then preserved in liquid nitrogen for at least 1 h. Sections (40

149 μm thick) of samples were cut with a Leica CM1850 cryostat at -20 °C using

150 deionized water as embedding medium to minimize possible effects of the embedding

151 medium on Zn speciation. To maintain the plant tissues intact and suitable for μ-XRF

152 analysis, the method developed by Lombi et al. was used.[30] Simply, a piece of Kapton

153 tape (3M, USA) was pressed on the top of the sample, with the blade of the

154 microtome cutting underneath. In this way, 40-μm thick sections were obtained

155 directly on the Kapton tape, and then a piece of Kapton tape was overcast on the other

156 side of the section as soon as possible. Sections were placed in the cryostat until

157 dryness and those in good condition were selected for μ-XRF mapping. For optical

158 fluorescence microscopic observation, 20 μm tissue sections of seedlings exposed to

159 100 mg ARS-ZnO NPs L^{-1} suspension, 10 mM ARS and deionized water were

160 prepared by the same method, but using optimum cutting temperature compound

161 (Tissue-Tek® O.C.T. Compound, Sakura Finetek, Torrance, CA) instead of deionized

162 water.

163 **2.4. Synchrotron X-ray absorption spectrum and μ-XRF microprobe analysis**

164 For the XAS analysis, the fresh maize seedings were first preserved in liquid nitrogen,

165 and then lyophilized at -40 °C for 48 h. 0.0300 g samples of lyophilized powder of

166 roots or shoots of maize seedlings exposed to 100 mg ZnO NPs L^{-1} or 30 mg Zn^{2+} L^{-1}

167 were pressed into pellets. The pellets were pasted on Kapton tape (3M, USA) and then

168 subjected to XAS analysis. Zinc K-edge X-ray absorption spectra were collected at

169 room temperature at the 1W1B beamline of the Beijing Synchrotron Radiation

170 Facility (Beijing, China). The energy of the Zn K-absorption edge (9659 eV) was

171 calibrated with Zn foil, and an energy range of -200-800 eV from the K-edge of Zn

172 was used to acquire the spectra. ZnO NPs, Zn phosphate (hopeite), Zn phytate,

173 Zn-sorbed hydroxylapatite (Zn_{ads}-Phos) to represent amorphous Zn phosphate,[31] ZnS,

174 Zn citrate, Zn malate and $ZnSO_4$ aqueous solution were used as reference compounds.

175 Data for the samples and liquid reference compounds were collected in fluorescence

176 mode under ambient conditions, and those for the solid reference compounds were

177 collected in transmission mode. Two to three scans were performed on average to

178 achieve an adequate signal/noise ratio. Standard XAFS data reduction procedures

179 were undertaken using the program package IFEFFIT[32] and WinXAS v 3.1[33] was

180 used for EXAFS fitting. The XANES data (average of two or three scans) of the

181 samples were analyzed by linear combination fitting (LCF) using Athena software.[34]

182 More detailed information about data analysis is provided in the ESI.

183 Synchrotron μ-XRF microprobe maps of 40 μm cross and longitudinal sections

184 prepared as described above were performed at room temperature at beamline 15U at

185 the Shanghai Synchrotron Radiation Facility (SSRF). Incident X-rays of 10.02 keV

186 were used to excite elements in the prepared samples. The electron energy in the

187 storage ring was 3.5 GeV with a current ranging from 120 to 210 mA. The

188 microfocused beam of about 10 μm was provided by a K-B lens with the sample at 45°

189 to the incident X-ray beam. The fluorescence yield was detected using a 7-element Si

190 (Li) solid state detector (E2V Scientific Instruments Ltd.) positioned at 90° to the

191 beam line. Dwell time per point was 1 s and the step size was set to 15 μm to 25 μm

192 depending on the size of the area mapped. The fluorescence intensities of Zn, K, Ca,

193 Fe, Mn, Cu and Compton scattering were recorded simultaneously. The fluorescence

194 intensity was normalized by I_0 and dwell time to correct for the effect of synchrotron

195 radiation beam flux variation on signal intensity. More detailed information about

196 data analysis is provided in the ESI.

197 **2.5. Fluorescence tracking and TEM analysis**

198 10 mM ZnO NPs stored in citrate buffer (100 mM, pH 6.5) were mixed with Alizarin

199 red S (50 mM) and shaken at 100 rpm for 24 h at room temperature, then the samples

200 were centrifuged at 20000 g for 1 h. The supernatants were discarded and the residues

201 were washed with deionized water until the supernatants were almost colorless. The

202 residues were retained, lyophilized and ground. Purple powder was obtained as

203 Alizarin red S labeled ZnO NPs (ARS-ZnO NPs). Maize seedlings were exposed to a

204 suspension of 100 mg L^{-1} ARS-ZnO NPs and a solution of 10 mM ARS. Fluorescence

205 microscopic images of different sections of plant tissues were observed using an

206 inverted phase-contrast fluorescence microscope (Zeiss Axiovert 200, Germany).

207 To image the cellular localization of ZnO NPs in root cells, tissue sections of

208 maize exposed to solutions with and without ZnO NPs were prepared by fixation,

209 gradual dehydration, embedment, polymerization, and ultrathin sectioning (70 nm),

210 and were stained and examined by TEM (JEOL JEM 1010, Tokyo, Japan). Method

211 details are provided in the ESI.

212

213 **3. Results**

3.1. ZnO nanoparticle characterization.

The purity of ZnO NPs (no surface coating) used in this study was 99.9 % with surface area of $29 \pm 1 \, m^2 \, g^{-1}$. XRD patterns revealed that the crystalline phase of the ZnO nanoparticles was consistent with zincite. TEM micrographs indicated that the primary ZnO NPs were nearly spherical with diameters of 30 ± 5 nm, obtained by measuring over 200 single particles. The isoelectric point (IEP) of ZnO NPs is 9.1 ± 0.2, indicative of positive surface charges at neutral pH. Dynamic light scattering analysis indicated that ZnO NPs tended to aggregate and exhibited a mean hydrodynamic diameter of around 450 nm with a wide range (Fig. S1 in the ESI).

3.2. Accumulation of Zn in maize under exposure to ZnO NPs

Dissolution of ZnO NPs at various concentrations over 24 h with and without plant exposure was measured first. As shown in Fig. 1A, the concentrations of dissolved Zn^{2+} increased with increasing particle density of ZnO NPs in the hydroponic medium in both cases, but much higher Zn^{2+} concentrations were detected in the presence of plants, especially at high particle densities (Fig. S2). Then comparative plant accumulation experiments were conducted by parallel exposure of maize to ZnO NPs and Zn^{2+}. After 7 d of exposure, the concentrations of Zn in roots and shoots increased quickly with increasing concentrations of Zn^{2+} or ZnO NPs below 5mg L^{-1} (dissolved Zn), followed by an apparent steady state in shoots and a slow increase in roots (Fig. 1B). It is interesting to note that shoot Zn concentrations under exposure to ZnO NPs and Zn^{2+} overlapped each other when the dissolved Zn^{2+} concentrations calculated based on the dissolution ratios of ZnO NPs at different particle densities were considered. Root Zn concentrations under the two treatments were also similar to each other, but differences were present in the treatments with ZnO NPs at high particle densities.

10

239   **3.3. Speciation of Zn in maize under exposure to ZnO NPs**

240   XAS analysis was conducted to elucidate Zn speciation in roots and shoots of

241   maize seedlings exposed to 30 mg L^{-1} (Zn concentration) ZnSO$_4$ and 100 mg ZnO

242   NPs L^{-1} (dissolved Zn 31.4 ± 1.7 mg L^{-1}). The Zn K-edge XANES and EXAFS

243   spectra of the reference compounds and the plant samples are shown in Fig. 2. The

244   LCF was performed on the XANES spectra of the samples (Fig. 2D) using the spectra

245   of Zn phosphate species including Zn hopeite and Zn$_{ads}$-Phos, considering their

246   similarity to the main features of the XAS spectra of the plant samples. Phytate Zn

247   was not included because it shares identical XAS spectra with hopeite (Fig. 2A, B, C).

248   [35] Standard spectra of other compounds among the reference chemicals were then

249   added in the fitting, respectively. However, only the addition of the spectra of ZnO

250   significantly improved the quality of fit (the normalized sum of square values

251   decreased by at least 10%). The LCF results (Table S1) showed a high proportion

252   (76-95 %) of zinc phosphate complexes (in both inorganic and organic forms) present

253   in the plant samples, with zinc phosphate (hopeite or Zn phytate) as the major species

254   in shoots (70-83%) and Zn$_{ads}$-Phos in roots (69-76%), respectively. The percentage of

255   ZnO(H) in roots (24%) treated with ZnO NPs was over four times more than that in

256   the other plant samples (Table S1).

257   **3.4. Distribution of Zn in maize under exposure to ZnO NPs**

258   Synchrotron μ-XRF microprobe mapping, which enables direct in situ quantitative

259   visualization of elemental distribution in plant tissues, was employed to observe the

260   spatial distribution of Zn in maize. Fig. 3 shows the distribution of Zn in root, stem,

261   and leaf cross-sections (optical photographs are provided in Fig. S3) of maize exposed

262   to 30 mg L^{-1} ZnSO$_4$ or 100 mg ZnO NPs L^{-1} (dissolved Zn 31.4 ± 1.7 mg L^{-1}). The

263   μ-XRF maps displayed distinct similarities in both distribution and content of Zn in

11

264   the leaves and stems under the two treatments (comparison between Fig. 3A and 3D,

265   and between 3B and 3E). However, more hot points (representing Zn accumulation)

266   in root cortex were found for the treatment with ZnO NPs than that with Zn^{2+} (Fig. 3C

267   and F).

268   **3.5. Localization of nanoparticles in maize**

269   Fluorescence labeling and TEM imaging were used to investigate the localization of

270   nanoparticles in maize. Alizarin red S (ARS) has been used as a fluorescent marker

271   for many metal oxide NPs,[35] and ARS-labeled TiO_2 NPs have been further

272   successfully used to track the translocation of TiO_2 NPs in both cancer cells and

273   plants.[15, 36] Therefore, ARS-labeled ZnO NPs (ARS-ZnO NPs) were prepared to track

274   the distribution of ZnO NPs inside maize. These ARS-ZnO NPs aggregates appeared

275   purple when observed with the naked eye and emitted bright orange fluorescence

276   using a violet filter (excitation wavelength 395-415 nm), while ARS alone that

277   accumulated in the roots displayed a purple color (Fig. S4). As shown in Fig. 4, the

278   blue color represented the background autofluorescence of plant tissues, while

279   ARS-ZnO NPs and their aggregates appeared as light orange dots (indicated by

280   arrows). Numerous light orange particles adhered to the root surface of maize after

281   exposure to ARS-ZnO NPs (Fig. 4A), indicating a strong affinity of ARS-ZnO NPs

282   for the root surface. In order to track the translocation of ARS-ZnO NPs inside maize,

283   both 20 μm cross and longitudinal sections of roots were imaged. Orange dots of

284   different sizes were observed inside the epidermis and cortex but none was observed

285   in the root vascular systems (Fig. 4B and C). However, a much higher intensity of

286   orange color appeared at the primary root-lateral root junction than in other regions

287   (Fig. 4D-I). Furthermore, none was observed in the shoots (Fig. S4).

288   Fig. 5 gives the TEM images of root sections in different zones after maize was

289   exposed to 100 mg L^{-1} ZnO NPs. Integrated cellular structures with no obvious dense

290   dots were observed in the roots without exposure to ZnO NPs (Fig. 5A). However,

291   copious dense dots were observed in the intercellular spaces and cells in the primary

292   root-lateral root junction areas (Fig. 5B) and these were confirmed to be

293   Zn-containing NPs by energy dispersive X-ray spectrometry (EDS) (Fig. S5). These

294   NPs and their aggregates were also observed in the surface and epidermis of roots

295   (Fig. S6). In addition, Zn-containing dense dots were also present in apoplast,

296   cytoplasm, membrane and vacuoles of some intact cells in the root tips (Fig. 5C and

297   Fig. S7), and even in the nuclei of cells with broken nuclear membranes (Fig. 5D) but

298   were absent from the nuclei of cells with intact nuclear membranes (Fig. 5C and Fig.

299   S7B). Zn-containing dense dots were observed in the cells of maturation zones of

300   roots, but their intensity was much weaker than that of root tips, with the exception of

301   the primary root-lateral root junction areas (Fig. S8).

302   ## 4. Discussion

303   The overlap in Zn contents in plant tissues vs dissolved Zn^{2+} concentration in ZnO NP

304   and ZnSO$_4$ treatments (Fig. 1) reveals that Zn accumulation in maize was mainly

305   determined by the actual Zn^{2+} concentration in the exposure suspensions. This

306   conclusion was also supported by the evidence of the great similarity in both the in

307   situ quantitative Zn distribution and Zn speciation in plant tissues (especially in shoots)

308   obtained from μ-XRF maps (Fig. 3) and the Zn K-edge XANES and EXAFS spectra

309   (Fig. 2) of maize seedlings exposed to ZnO NPs and Zn^{2+}.

310   Synchrotron XAS analysis of the bulk plant samples indicates that Zn phosphate

311   complexes were the major Zn species in all the plant samples. Previous studies have

312   found the conversion of Zn^{2+} ions to Zn phosphate in *Arabidopsis* grown

313   hydroponically.[35, 37-39] More recently, transformation of ZnO to Zn phosphate in

314   wheat exposed to Zn NPs in a sand matrix has also been reported.[40] Nevertheless,

315   differences in Zn coordinate structures between maize roots and shoots were found in

316   the present study. Zn was present in a form more similar to amorphous Zn phosphate

317   (Zn_{ads}-Phos) in roots, while Zn phosphate (hopeite or Zn phytate) was the major Zn

318   species in shoots. Zhao et al. suggested that the formation of Zn phosphate in

319   *Arabidopsis halleri* roots was mainly due to the co-precipitation of Zn and PO_4^{3-} on

320   the rhizodermis, while Zn phosphate was not found in shoots.[38] Our results further

321   confirm that the Zn phosphate species stored in maize roots was poorly crystallized,

322   possibly due to the low PO_4^{3-} concentration in the exposure suspension (0.01 mmol

323   L^{-1}). In contrast to Zn speciation in the roots, Zn accumulated in maize shoots mainly

324   as hopeite/Zn phytate-like species. Hopeite is unlikely to be the main form in plant

325   shoots because of the low PO_4^{3-} concentration in shoots. Therefore, it is reasonable to

326   speculate that Zn phytate was likely the main species present in maize shoots because

327   phytic acid (*myo*-inositol *kis*-hexaphosphate) is an effective chelator of cations such

328   as calcium, zinc and iron,[41] and maize is among the cereal grains with high contents

329   of phytic acid.[42] However, the presence of hopeite cannot be excluded because of

330   method limitations. Differences in Zn speciation between the Zn^{2+} and ZnO NP

331   treatments were only found in root samples with higher ZnO(H) percentage in roots

332   treated with ZnO NPs, likely attributable to root surface adsorption of ZnO NPs and

333   partial internalization of ZnO NPs in roots, as evidenced by fluorescent tracking and

334   TEM. Whether or not those ZnO NPs internalized in roots can be transformed to Zn

335   phosphate species inside maize during root-to-shoot transport needs further

336   investigation.

337   Although it has been confirmed that Zn^{2+} from dissolution of ZnO NPs was the

338   main (or perhaps the sole) source of Zn for maize uptake under treatment with ZnO

339 NPs, we still cannot rule out the possibility of the entry and translocation of ZnO NPs

340 in maize. ARS-labeled ZnO NPs (ARS-ZnO NPs) were used to track the distribution

341 of ZnO NPs inside plants, which can provide macroscopic uptake and transport

342 pathways of NPs in plants. In order to check whether the observed orange dots in

343 plants were ARS-ZnO NPs or their aggregates, we examined the free ARS

344 accumulated in roots. The free ARS appeared as purple color, which was much

345 different from the color of ARS-ZnO NPs (Fig. S4). In addition, the content of the

346 released dye from ARS-ZnO NPs in the exposure suspension was very limited (Fig.

347 S9), therefore the potential influence of fluorescence emitted by plant uptake of free

348 ARS and its complexation with calcium was negligible. ARS-ZnO NPs were observed

349 inside the epidermis and cortex, but none was observed in the root vascular systems

350 (Fig. 4B and C). This observation suggests that maize roots took up the ARS-ZnO

351 NPs, but the endodermis prevented their entry into the root vascular systems.

352 However, there was an interesting phenomenon that a much higher intensity of orange

353 color was observed at the primary root-lateral root junction compared with other

354 regions (Fig. 4 D-I). At this specific location, ARS-ZnO NPs were even observed in

355 the vascular cylinder of taproots (Fig. 4I), similar to the observation of FITC-stained

356 ZnO NPs by Zhao et al..[27] Consistent observations were also obtained for bare ZnO

357 NPs with μ-XRF mapping, which showed a much higher Zn accumulation in this area

358 than in the others (Fig. 6). TEM images further showed the presence of numerous

359 Zn-containing dense dots in the intercellular space and cells of the primary root-lateral

360 root junction (Fig. 5B). Both the speciation analysis by XAFS and fluorescence

361 labeling suggest that these dots shared the same features of ZnO NPs. In the mature

362 zone of the roots, lignified cells left large vacant spaces for localization of NPs, and

363 the abundant vessels of different sizes in the xylem provided available channels for

15

364   the uptake of NPs with water flow. However, the Casparian strip, located in the

365   transverse and radial walls of endodermal cells, forms a barrier to prevent the entry of

366   macromolecules and particles into the vascular cylinder.[43] Therefore, the formation of

367   the xylem-Casparian strip is the key barrier for the entry of ZnO NPs. As shown in

368   Fig. 4D and 4F, one terminal of the lateral root developed from the secondary xylem

369   was in contact with the vascular cylinder of the primary root where the Casparian strip

370   was disconnected (Fig. 4G and 4I),[44] thus providing an opportunity for NPs to

371   traverse the membrane. Lateral root transmission is therefore speculated to be a

372   plausible pathway for NPs to enter the vascular cylinder of the primary roots. TEM

373   images demonstrate the internalized ZnO NPs in root cells at the area of root tips in

374   maize after exposure to ZnO NPs. The main reason is that there is no exact

375   morphological differentiation, and a Casparian strip has not formed at the root tips.

376   Further, both growth and division of cells in this zone are rapid.[45] NPs adsorbed on

377   the surface of root tip cells were liable to be embedded in the intercellular space or

378   enveloped inside the cells along with their fast division and growth. At the root tips,

379   new cells are generated with root elongation. NPs internalized into surface cells were

380   subsequently embedded by the new cells and present in the cells of other root zones,

381   and thereby had the opportunity to further enter the vascular cylinder of the primary

382   roots through the junction regions of the primary root-lateral root. All results suggest

383   that disconnection of the Casparian strip at the primary root-lateral root junction and

384   an undeveloped Casparian strip combined with rapid cell growth and division at the

385   root tips open a possible entry door for NPs at these specific locations.

386   No NPs were observed in maize shoots in this study by fluorescent tracking (Fig.

387   S4D, E) or TEM imaging (Fig. S8C, D). Although there is a lack of substantial

388   evidence to support or reject the upward translocation of ZnO nanoparticles in shoots

389   due to methodological limitations, it is certain that the quantity of ZnO NPs entering

390   the aerial parts of maize was very low if not zero. On the other hand, it would be

391   expected that if some ZnO NPs enter plant roots they will be liable to undergo

392   biotransformation to form Zn phosphate (mainly as Zn phytate) on their long-range

393   upward transport pathway, an assertion that was supported by the observation that Zn

394   existed mainly as Zn phosphate in the plant tissues. Such biotransformation will, as a

395   result, prevent the upward translocation of ZnO NPs inside maize.

396   **5. Conclusions**

397   A comprehensive uptake pathway of ZnO NPs in maize is demonstrated based on

398   observations from a combination of microscopic and spectroscopic techniques. Some

399   of the ZnO NPs underwent dissolution in the exposure medium, which was enhanced

400   as the result of root metabolic activities. The Zn^{2+} ions released from ZnO NPs were

401   taken up by roots and accumulated in maize tissues mainly as Zn phosphate in both

402   inorganic and organic forms. This is the main pathway for Zn uptake by maize.

403   Simultaneously, a small fraction of ZnO NPs adsorbed on root surfaces enter root

404   cortex due to rapid cell division and elongation of the root tips, some of which enter

405   the vascular systems through the gaps of the Casparian strip at the sites of the primary

406   root-lateral root junction. Biotransformation of the ZnO NPs to Zn phosphate inside

407   plants further limits their long-distance transport, resulting in negligible upward

408   translocation of ZnO NPs into the shoots. Whether or not this nanoparticle uptake

409   pathway that we propose is applicable to other nanoparticles and in soil-plant system

410   may merit further investigation. The results of this study highlight the importance of

411   dissolution of ZnO NPs and the uptake of Zn^{2+} by plants, which indicates that our

412   knowledge of plant uptake and phytotoxicity of Zn can to a large extent explain the

413   interactions between ZnO NPs and plants.

References

1 M. R. Wiesner, G. V. Lowry, P. Alvarez, D. Dionysiou and P. Biswas, *Environ Sci Technol*, 2006, 40, 4336-4345.

2 S. J. Klaine, P. J. J. Alvarez, G. E. Batley, T. F. Fernandes, R. D. Handy, D. Y. Lyon, S. Mahendra, M. J. McLaughlin and J. R. Lead, *Environ Toxicol Chem*, 2008, 27, 1825-1851.

3 A. Nel, T. Xia, L. Madler and N. Li, *Science*, 2006, 311, 622-627.

4 E. Navarro, A. Baun, R. Behra, N. B. Hartmann, J. Filser, A. J. Miao, A. Quigg, P. H. Santschi and L. Sigg, *Ecotoxicology*, 2008, 17, 372-386.

5 X. M. Ma, J. Geiser-Lee, Y. Deng and A. Kolmakov, *Sci Total Environ*, 2010, 408, 3053-3061.

6 R. Nair, S. H. Varghese, B. G. Nair, T. Maekawa, Y. Yoshida and D. S. Kumar, *Plant Sci*, 2010, 179, 154-163.

7 T. Sabo-Attwood, J. M. Unrine, J. W. Stone, C. J. Murphy, S. Ghoshroy, D. Blom, P. M. Bertsch and L. A. Newman, *Nanotoxicology*, 2012, 6, 353-360.

8 Z. Y. Wang, X. Y. Xie, J. Zhao, X. Y. Liu, W. Q. Feng, J. C. White and B. S. Xing, *Environ Sci Technol*, 2012, 46, 4434-4441.

9 J. E. Canas, M. Q. Long, S. Nations, R. Vadan, L. Dai, M. X. Luo, R. Ambikapathi, E. H. Lee and D. Olszyk, *Environ Toxicol Chem*, 2008, 27, 1922-1931.

10 S. Asli and P. M. Neumann, *Plant Cell Environ*, 2009, 32, 577-584.

439   11   X. M. Tan, C. Lin and B. Fugetsu, *Carbon*, 2009, 47, 3479-3487.

440   12   K. Birbaum, R. Brogioli, M. Schellenberg, E. Martinoia, W. J. Stark, D. Gunther

441   and L. K. Limbach, *Environ Sci Technol*, 2010, 44, 8718-8723.

442   13   J. A. Hernandez-Viezcas, H. Castillo-Michel, A. D. Servin, J. R. Peralta-Videa

443   and J. L. Gardea-Torresdey, *Chem Eng J*, 2011, 170, 346-352.

444   14   N. C. Carpita and D. M. Gibeaut, *Plant J*, 1993, 3, 1-30.

445   15   J. Kurepa, T. Paunesku, S. Vogt, H. Arora, B. M. Rabatic, J. J. Lu, M. B. Wanzer,

446   G. E. Woloschak and J. A. Smalle, *Nano Lett*, 2010, 10, 2296-2302.

447   16   S. J. Lin, J. Reppert, Q. Hu, J. S. Hudson, M. L. Reid, T. A. Ratnikova, A. M.

448   Rao, H. Luo and P. C. Ke, *Small*, 2009, 5, 1128-1132.

449   17   R. Chen, T. A. Ratnikova, M. B. Stone, S. Lin, M. Lard, G. Huang, J. S. Hudson

450   and P. C. Ke, *Small*, 2010, 6, 612-617.

451   18   H. Zhu, J. Han, J. Q. Xiao and Y. Jin, *J Environ Monitor*, 2008, 10, 713-717.

452   19   E. Corredor, P. S. Testillano, M. J. Coronado, P. Gonzalez-Melendi, R.

453   Fernandez-Pacheco, C. Marquina, M. R. Ibarra, J. M. de la Fuente, D. Rubiales,

454   A. Perez-De-Luque and M. C. Risueno, *BMC Plant Biol*, 2009, 9, 45-53.

455   20   A. Hischemoller, J. Nordmann, P. Ptacek, K. Mummenhoff and M. Haase, *J

456   Biomed Nanotechnol*, 2009, 5, 278-284.

457   21   N. Geldner, D. Roppolo, B. De Rybel, V. D. Tendon, A. Pfister, J. Alassimone, J.

458   E. M. Vermeer, M. Yamazaki, Y. D. Stierhof and T. Beeckman, *Nature*, 2011, 473,

459   380-384.

460   22   C. M. Rico, S. Majumdar, M. Duarte-Gardea, J. R. Peralta-Videa and J. L.

461   Gardea-Torresdey, *J Agr Food Chem*, 2011, 59, 3485-3498.

462   23   D. X. Zhou and A. A. Keller, *Water Res*, 2010, 44, 2948-2956.

463   24   F. Gottschalk, T. Sonderer, R. W. Scholz and B. Nowack, *Environ Sci Technol*,

464   2009, 43, 9216-9222.

465 25 D. H. Lin and B. S. Xing, *Environ Sci Technol*, 2008, 42, 5580-5585.

466 26 M. L. Lopez-Moreno, G. de la Rosa, J. A. Hernandez-Viezcas, H.

467   Castillo-Michel, C. E. Botez, J. R. Peralta-Videa and J. L. Gardea-Torresdey,

468   *Environ Sci Technol*, 2010, 44, 7315-7320.

469 27 L. J. Zhao, J. R. Peralta-Videa, M. H. Ren, A. Varela-Ramirez, C. Q. Li, J. A.

470   Hernandez-Viezcas, R. J. Aguilera and J. L. Gardea-Torresdey, *Chem Eng J*,

471   2012, 184, 1-8.

472 28 J. A. Hernandez-Viezcas, H. Castillo-Michel, J. C. Andrews, M. Cotte, C. Rico, J.

473   R. Peralta-Videa, Y. Ge, J. H. Priester, P. A. Holden and J. L. Gardea-Torresdey,

474   *ACS Nano*, 2013, 7, 1415-1423.

475 29 Y. Yu, H. L. Huang, L. Luo, B. Wen and S. Z. Zhang, *J Agr Food Chem*, 2009,

476   57, 3695-3701.

477 30 E. Lombi, K. G. Scheckel, J. Pallon, A. M. Carey, Y. G. Zhu and A. A. Meharg,

478   *New Phytol*, 2009, 184, 193-201.

479 31 G. Sarret, G. Willems, M. P. Isaure, M. A. Marcus, S. C. Fakra, H. Frerot, S.

480   Pairis, N. Geoffroy, A. Manceau and P. Saumitou-Laprade, *New Phytol*, 2009,

481   184, 581-595.

482 32 M. Newville, *J Synchrotron Radiat*, 2001, 8, 322-324.

483 33 T. Ressler, *J Synchrotron Radiat*, 1998, 5, 118-122.

484 34 T. Rajh, L. X. Chen, K. Lukas, T. Liu, M. C. Thurnauer and D. M. Tiede, *J Phys

485   Chem B*, 2002, 106, 10543-10552.

486 35 G. Sarret, P. Saumitou-Laprade, V. Bert, O. Proux, J. L. Hazemann, A. S.

487   Traverse, M. A. Marcus and A. Manceau, *Plant Physiol*, 2002, 130, 1815-1826.

488 36 K. T. Thurn, T. Paunesku, A. G. Wu, E. M. B. Brown, B. Lai, S. Vogt, J. Maser,

20

489   M. Aslam, V. Dravid, R. Bergan and G. E. Woloschak, *Small*, 2009, 5,

490   1318-1325.

491   37   H. Kupper, E. Lombi, F. J. Zhao and S. P. McGrath, *Planta*, 2000, 212, 75-84.

492   38   F. J. Zhao, E. Lombi, T. Breedon and S. P. McGrath, *Plant Cell Environ*, 2000,

493   23, 507-514.

494   39   G. Sarret, J. Vangronsveld, A. Manceau, M. Musso, J. D'Haen, J. J. Menthonnex

495   and J. L. Hazemann, *Environ Sci Technol*, 2001, 35, 2854-2859.

496   40   C. O. Dimkpa, D. E. Latta, J. E. McLean, D. W. Britt, M. I. Boyanov and A. J.

497   Anderson, *Environ Sci Technol*, 2013, 47, 4734-4742.

498   41   V. Raboy, K. A. Young, J. A. Dorsch and A. Cook, *J Plant Physiol*, 2001, 158,

499   489-497.

500   42   C. L. Adams, M. Hambidge, V. Raboy, J. A. Dorsch, L. Sian, J. L. Westcott and

501   N. F. Krebs, *Am J Clin Nutr*, 2002, 76, 556-559.

502   43   I. Karahara, A. Ikeda, T. Kondo and Y. Uetake, *Planta*, 2004, 219, 41-47.

503   44   M. Mccully, *Plant Physiol*, 1995, 109, 1-6.

504   45   S. Doncheva, *J Plant Physiol*, 1998, 153, 482-487.

505   46   E. Wild and K. C. Jones, *Environ Sci Technol*, 2009, 43, 5290-5294.

506

507

508 **Figure legends**

509

510 **Fig. 1** Comparative dissolution of ZnO NPs with and without plants over 24 h (A); Zn

511 accumulation in shoots and roots of maize exposed to Zn^{2+} and ZnO for 7 days (B);

512 soluble Zn in B represents the dissolved concentrations of Zn^{2+} released from ZnO

513 NPs.

514

515 **Fig. 2** Normalized Zn K-edge XANES spectra (A) , k^3-weighted EXAFS data (B) and

516 corresponding radial distribution functions (RDF) obtained by Fourier transformation

517 of the EXAFS spectra (C) of the model compounds; normalized Zn K-edge XANES

518 spectra (D), k^3-weighted EXAFS data (E) and corresponding radial distribution

519 functions (RDF) obtained by Fourier transformation of the EXAFS spectra (F) of

520 plant samples; solid lines represent experimental data, dashed lines represent fitted

521 data.

522

523 **Fig. 3** Synchrotron μ-XRF microprobe imaging of Zn in leaf, stem, and root material

524 of maize seedlings exposed to 30 mg Zn^{2+} L^{-1} (A, B, C) and 100 mg ZnO NPs L^{-1} (D,

525 E, F), respectively; scale bars represent 500 μm. The fluorescence yield counts

526 collected were normalized by I_0 and dwell time. The red color was scaled to the

527 maximum elemental concentration value for each map and the blue color was scaled

528 to the minimum.

529

530 **Fig. 4** Optical fluorescence microscopy images of ARS-ZnO NP adsorption on the

531 root surface (A); the cross sections (B, D, G) and longitudinal sections (C, E, F, H, I)

532 of maize roots exposed to ARS-ZnO NPs ; G, H, I are enlargements of the panes in D,

533   E, F, respectively; exodermis (ex), cortex (co), endodermis (en) and vascular system

534   (vs) are shown in B and C.

535

536   **Fig. 5** TEM images of root tip sections of maize seedlings treated in blank (A) and

537   primary root-lateral root junction of maize treated with 100 mg L^{-1} ZnO NPs (B),

538   intact (C) and injured (D) cells in root tip sections under 100 mg L^{-1} ZnO NPs

539   treatment; insert is enlargement of the pane in each figure.

540

541   **Fig. 6** Synchrotron μ-XRF mapping of longitudinal (A) and cross (B) sections of

542   maize root exposed to ZnO NPs, which reveal that a high level of Zn has accumulated

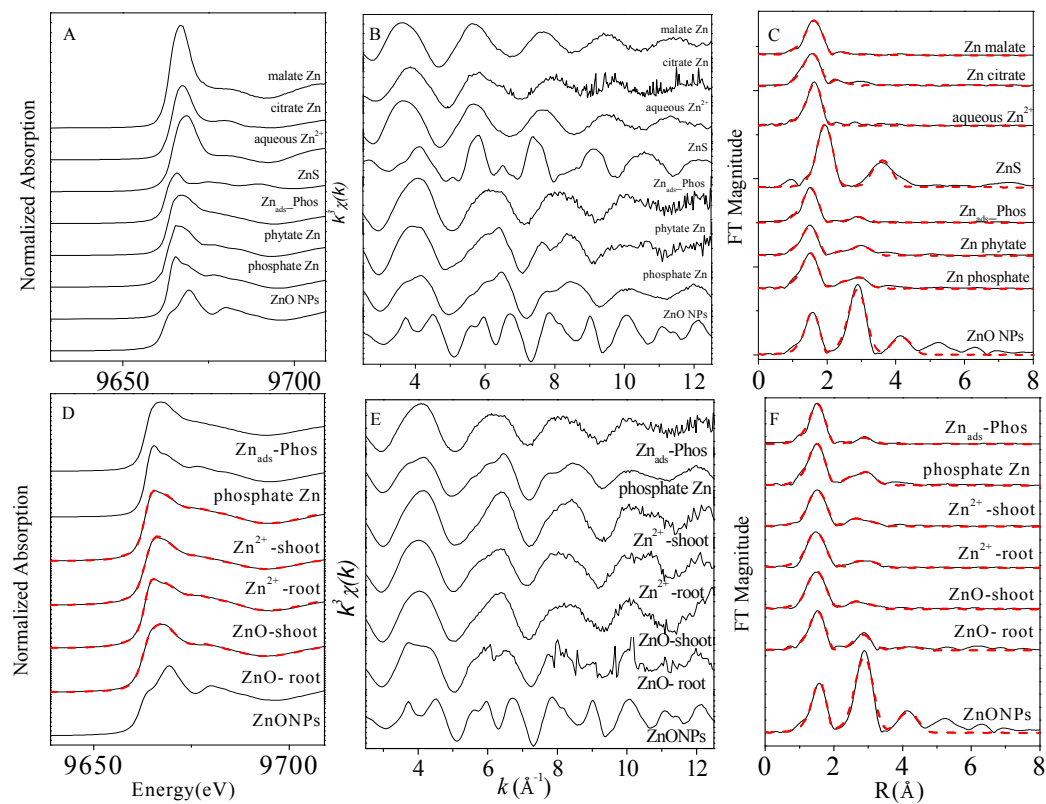543   in the area of the primary root-lateral root junction; bars represent 500 μm.
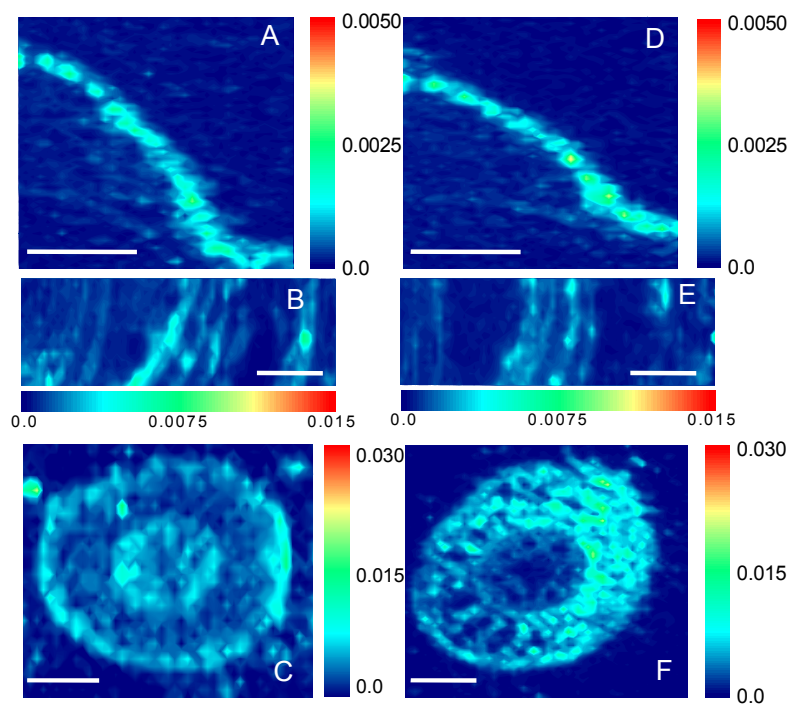
544

545

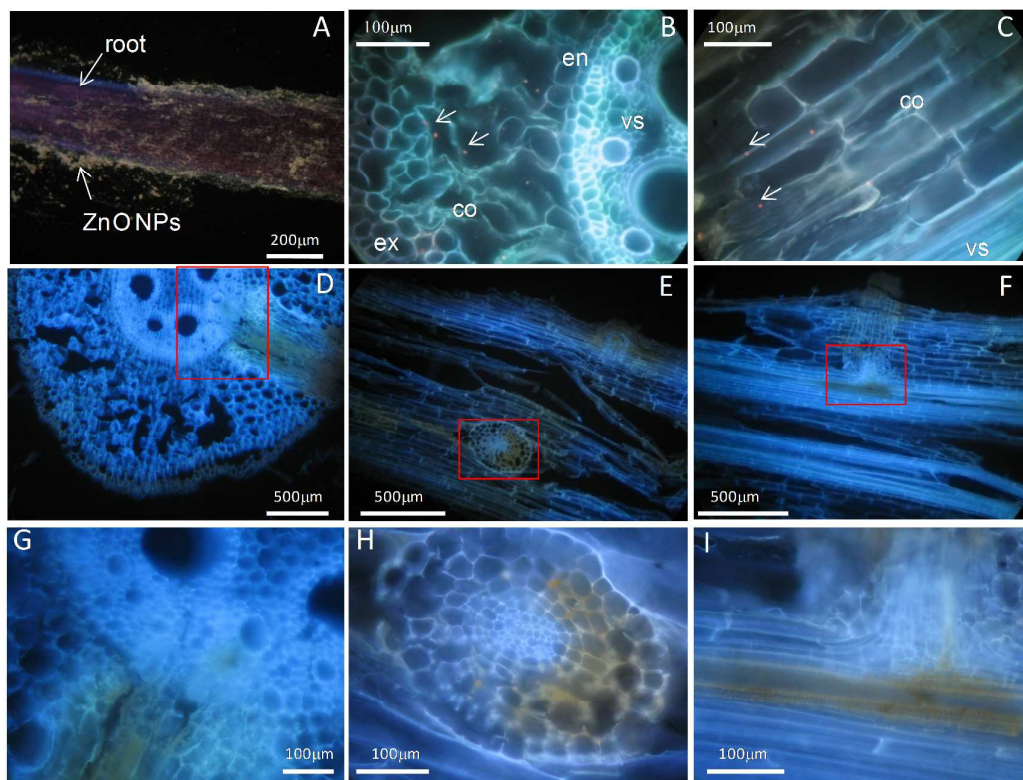546   **Fig. 1**

547
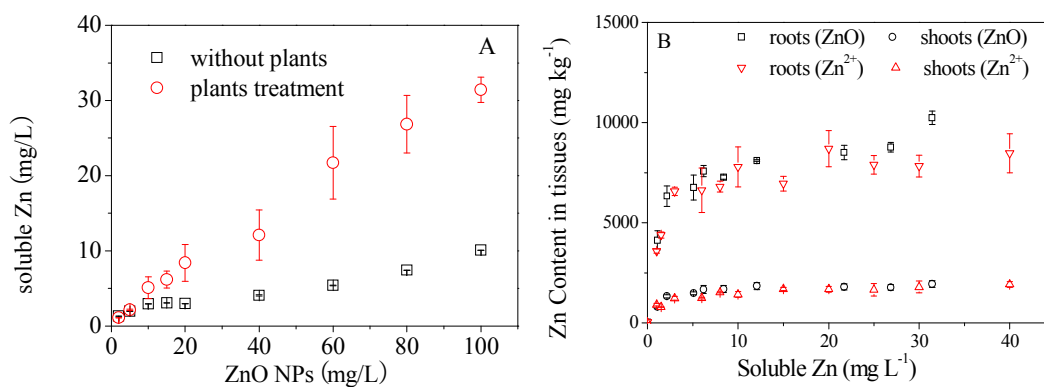
548

549   **Fig. 2**

550

551   **Fig. 3**
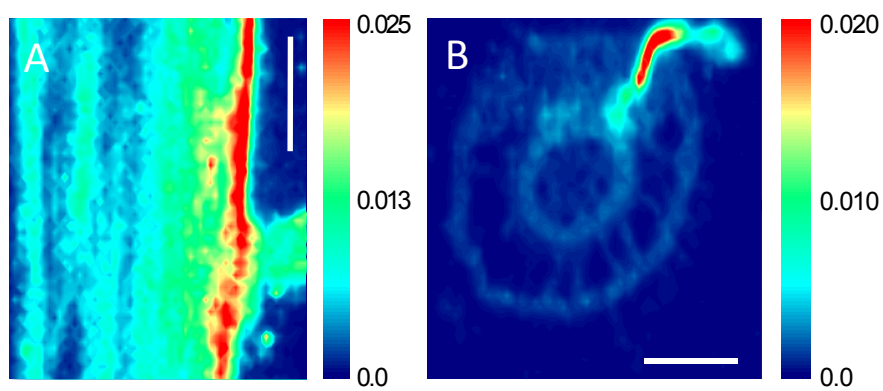

552

553   **Fig. 4**

554

555

556

Fig. 5

557

558

Fig. 6

559

26